Advances in Mathematical Sciences and Applications Vol. 29, No. 1 (2020), pp. 129–143



# MATHEMATICAL MODEL FOR HUMAN MITRAL VALVE

#### QIAN YANG

School of Sciences, Xi'an University of Technology, Xi'an, 710054, China (E-mail: yq931122@sina.com)

#### XIAOQIN SHEN \*

School of Sciences, Xi'an University of Technology, Xi'an, 710054, China (E-mail: xqshen@xaut.edu.cn)

#### JUNJUN JIA, TIANTIAN WANG

School of Sciences, Xi'an University of Technology, Xi'an, 710054, China (E-mail: 1164395007@qq.com, 275603528@qq.com)

and

#### LI CAI

NPU-UoG International Cooperative Lab for Computation & Application in Cardiology, Northwestern Polytechnical University, Xi'an, 710072, China (E-mail: caili@nwpu.edu.cn)

**Abstract.** We apply a mathematical elastic shell model to describe a human mitral valve based on its geometric and mechanical properties. Specifically, we adopt an elliptic variational model called Koiter's equation to simulate the human mitral valve. Then, we provide a conforming finite element method to compute the deformation of the mitral valve. The numerical results show that the proposed mathematical model simulates well the human mitral valve.

Communicated by Michel Chipot; Received January 7, 2020.

This work is supported by the National Natural Science Foundation of China (Nos. 11971379, 11571275, 11871399) and by the Natural Science Foundation of Shaanxi Province (No. 2018JM1014).

AMS Subject Classification: 65N12, 65N15, 65N30.

Keywords: mitral valve, Koiter's model, finite element method, HCT element.

<sup>\*</sup>Corresponding author

# 1 Introduction

As one of the important valve tissues in the human heart, the mitral valve guarantees the one-way flow of blood from the left atrium to the left ventricle, and plays an important role in maintaining the normal function of the heart [1]. So far, the research on the modeling of the mitral valve can be divided into structural models and fluid-solid coupling models. Structure models only consider the structure and shape of the mitral valve, and are the foundation of fluid-structure-interaction models. Weinberg and Kaazempur-Mofrad [2, 3] used finite element simulation to describe the three-dimensional stress and strain of a mitral valve undergoing large deformations. Prot's et al. [4] conducted a finite element analysis of the effect of the ring shape and tendine-cord force distribution of the mitral valve on the whole human heart. Dal Pan F's et al. [5] established a finite element model for the mitral valve, and simulated the mitral diastole by an edge suture method.

A fluid-structure-interaction (FSI) model refers to a model exploring the interaction between the structure of a mitral valve and the fluid domain. Research in this field has been mainly done by Kunzelman's et al. [6, 7, 8], Lim's et al. [9], Einstein's et al. [10] and so on. For example, Kunzelman's et al. [6, 7, 8] established the most primitive human mitral valve model, and then simulated the mitral valve closing process based on the original model. Lim's et al. [9] built a flap with a uniform thickness of the membrane structure to simulate the normal working mechanism for a mitral valve, though the free edge of the flap had no tip, and local details of flap morphology were ignored in their model. Einstein's et al. [10] set up an FSI model of a mitral valve in the human heart, but oversimplified the geometric shape and the physiological structure of the mitral valve. A new structural finite element model is proposed by Marco et al. [11], considering the following: (i) an accurate morphological description of the valve, (ii) a description of tissues mechanical properties accounting for anisotropy and nonlinearity, (iii) dynamic boundary conditions of mimic annulus and papillary muscles contraction. In recent years, Luo et al. [13, 12, 14] also proposed a fluid-solid coupling model of a human mitral valve. Shen et al. [15, 16, 17] studied the geometry of a mitral valve, a pulmonary valve and a tricuspid valve respectively, and gave mathematical parametric equations for these valves, and came up with an elastic shell model for the human tricuspid valve.

As shown by medical imaging data, the leaflets of the human mitral valve are extremely thin, with a thickness of about 1.32mm (cf. [11]). The mitral valve is studied here using Koiter's shell model which is a well-recognized two-dimensional for thin elastic shells. Koiter [18, 19] defined the two-dimensional (2D) model to approximate three-dimensional elasticity for thin shells in the 1960s. Ciarlet [20] later defined different shell models based on Koiter's model according to the middle surface of shell. Bernadou [21] conducted a general analysis of the finite element methods (FEMs) to conforming, nonconforming and mixed finite elements for Koiter's model. In recent years. Shen et al. [22, 23, 24, 25, 26] presented several numerical computations of Koiter's model under some special assumptions.

In this paper, our aim is to employ a mathematical elastic shell model to describe the mitral valve elastic model. More specifically, we use Koiter's model for the mitral valve leaflets and propose a numerical approximation scheme for this elastostatics model. To this end, we discretize spatial variables. In other words, we use conforming finite elements

(linear triangles) to approximate the tangent components of the displacement, and another conforming finite element (HCT triangles) to approximate the normal component of the displacement. Thus, we define a mathematical model for the human mitral valve, perform numerical simulations and analyse the results. Hopefully, our research will provide a basis for the dynamic model and the functional simulation of the human mitral valve.

## 2 Mathematical model and numerical schemes

#### 2.1 Preliminaries

Our notation is generally that of [27]. In the following, Latin indices and exponents  $i, j, k, \dots \in \{1, 2, 3\}$ , whereas Greek indices and exponents  $\alpha, \beta, \gamma, \dots \in \{1, 2\}$ . Furthermore, the repeated index summation convention is used in a systematic way.

Let  $\omega$  be an open, bounded, connected subset of  $\mathbb{R}^2$ . Let the boundary  $\gamma = \partial \omega$  be Lipschitz-continuous, and let  $\gamma = \gamma_0 \cup \gamma_1$  be a partition of  $\gamma$  into two measurable subsets with  $\gamma_0 \cap \gamma_1 = \emptyset$ , where  $\gamma_0$  with length  $\gamma_0 > 0$  is the clamped boundary, and  $\gamma_1$  is the free boundary. Let  $y = (y_\alpha)$  denote a generic point in the closure  $\overline{\omega}$  of the set  $\omega$  and let  $\partial_\alpha := \partial/\partial y_\alpha$ . Consider an immersion  $\vec{\theta} \in C^3(\overline{\omega}; \mathbb{R}^3)$ , so the two vectors

$$\vec{a}_{\alpha}(y) := \partial_{\alpha} \vec{\theta}(y),$$

are linearly independent at all points  $y \in \overline{\omega}$  (cf. [28]). The two vectors span the tangent plane to the surface

$$S := \vec{\theta}(\overline{\omega})$$

at the point  $\vec{\theta}(y)$ , and the unit vector

$$\vec{a}_3(y) := \frac{\vec{a}_1(y) \times \vec{a}_2(y)}{|\vec{a}_1(y) \times \vec{a}_2(y)|}$$

is normal to S at point  $\vec{\theta}(y)$ . These vectors  $\vec{a}_i(y)$  constitute the covariant basis at the point  $\vec{\theta}(y)$ , whereas the vectors  $\vec{a}^i(y)$  is defined by the relations

$$\vec{a}^i(y) \cdot \vec{a}_j(y) = \delta^i_j$$

constitute the contravariant basis at point  $\vec{\theta}(y)$ , where  $\delta_j^i$  is the Kronecker symbol (note that  $\vec{a}^3(y) = \vec{a}_3(y)$  and that the vector  $\vec{a}^{\alpha}(y)$  is also in the tangent plane to S at  $\vec{\theta}(y)$ ).

 $a_{\alpha\beta}$  and  $a^{\alpha\beta}$  denote the covariant and contravariant components of the metric tensor of S respectively. They are defined by

$$a_{\alpha\beta} := \vec{a}_{\alpha} \cdot \vec{a}_{\beta}, \qquad a^{\alpha\beta} := \vec{a}^{\alpha} \cdot \vec{a}^{\beta}, \quad \vec{a}^{\alpha} = a^{\alpha\beta}\vec{a}_{\beta}.$$

 $b_{\alpha\beta}$  and  $b_\alpha^\beta$  denote the covariant and mixed components of the curvature tensor of S , and are defined by

$$b_{\alpha\beta} := \vec{a}^3 \cdot \partial_{\beta} \vec{a}_{\alpha}, \qquad b_{\alpha}^{\beta} := a^{\beta\sigma} \cdot b_{\sigma\alpha}.$$

The Christoffel symbols  $\Gamma^{\sigma}_{\alpha\beta}$  on S are defined by:

$$\Gamma^{\sigma}_{\alpha\beta} := \vec{a}^{\sigma} \cdot \partial_{\alpha} \vec{a}_{\beta}.$$

Note that

$$(a^{\alpha\beta}) = (a_{\alpha\beta})^{-1}.$$

The determinant of the metric tensor is denoted

$$a := \det(a_{\alpha\beta})$$

Finally, we introduce the two-dimensional elastic tensor along S through its contravariant components  $a^{\alpha\beta\sigma\tau}$  defined by

$$a^{\alpha\beta\sigma\tau} = \frac{4\lambda\mu}{\lambda + 2\mu} a^{\alpha\beta} a^{\sigma\tau} + 2\mu (a^{\alpha\sigma} a^{\beta\tau} + a^{\alpha\tau} a^{\beta\sigma}),$$

where  $\lambda \geq 0$ ,  $\mu > 0$  are the Lamé constants of the elastic material.

#### 2.2 Mathematical model

Koiter's equations[19] define a 2D model for a linearly elastic shell of the following form

$$\begin{cases}
Find \quad \vec{\zeta} \in \vec{V}_K(\omega) := \{\vec{\zeta} = (\zeta_i) \in H^1(\omega) \times H^1(\omega) \times H^2(\omega); \zeta_i = \partial_n \zeta_3 = 0 \text{ on } \gamma_0\}, \\
such that \quad \varepsilon \int_{\omega} a^{\alpha\beta\sigma\tau} \gamma_{\sigma\tau}(\vec{\zeta}) \gamma_{\alpha\beta}(\vec{\eta}) \sqrt{a} dy + \frac{\varepsilon^3}{3} \int_{\omega} a^{\alpha\beta\sigma\tau} \rho_{\sigma\tau}(\vec{\zeta}) \rho_{\alpha\beta}(\vec{\eta}) \sqrt{a} dy \\
= \int_{\omega} p^i \eta_i \sqrt{a} dy, \forall \vec{\eta} \in \vec{V}_K(\omega),
\end{cases} \tag{1}$$

where  $\varepsilon$  is the half-thickness of the shell,  $\partial_n \zeta_3$  denotes the outer normal derivative of  $\zeta_3$  along the boundary of  $\omega$ , and  $p^i \in L^2(\omega)$  are given functions accounting for the applied forces on the middle surface S. The unknown is the vector  $\vec{\zeta} = (\zeta_1, \zeta_2, \zeta_3)$  whose components  $\zeta_i$  are the covariant components of the displacement field  $\zeta_i \vec{a}^i$  of the middle surface S.

Here, the functions  $\gamma_{\alpha\beta}(\vec{\eta})$  and  $\rho_{\alpha\beta}(\vec{\eta})$  are the customary covariant components of the linearized change of metric and change of curvature tensors defined by

$$\gamma_{\alpha\beta}(\vec{\eta}) := \frac{1}{2} (\partial_{\beta}\eta_{\alpha} + \partial_{\alpha}\eta_{\beta}) - \Gamma^{\sigma}_{\alpha\beta}\eta_{\sigma} - b_{\alpha\beta}\eta_{3},$$

$$\rho_{\alpha\beta}(\vec{\eta}) := \partial_{\alpha\beta}\eta_{3} - \Gamma^{\sigma}_{\alpha\beta}\partial_{\sigma}\eta_{3} - b^{\sigma}_{\alpha}b_{\alpha\beta}\eta_{3}$$

$$+ b^{\sigma}_{\alpha}(\partial_{\beta}\eta_{\sigma} - \Gamma^{\tau}_{\beta\sigma}\eta_{\tau}) + b^{\tau}_{\beta}(\partial_{\alpha}\eta_{\tau} - \Gamma^{\sigma}_{\alpha\tau}\eta_{\sigma})$$

$$+ (\partial_{\alpha}b^{\tau}_{\beta} + \Gamma^{\tau}_{\alpha\sigma}b^{\sigma}_{\beta} - \Gamma^{\sigma}_{\alpha\beta}b^{\tau}_{\sigma})\eta_{\tau}.$$

Then, we have the following existence and uniqueness theorem for the problem (1) (cf. [17]).

**Theorem 2.1.** Let  $\omega$  be a bounded connected open subset in  $\mathbb{R}^2$ , whose boundary  $\gamma = \partial \omega$  is Lipschitz-continuous. Let  $\gamma_0$  be a non-empty relatively open subset of  $\gamma$  and let  $\vec{\theta} \in C^3(\bar{\omega}; \mathbb{R}^3)$  be an immersion. Then, problem (1) has one and only one solution.

*Proof.* With the notations,

$$a(\vec{\zeta}, \vec{\eta}) := \varepsilon \int_{\omega} a^{\alpha\beta\sigma\tau} \gamma_{\sigma\tau}(\vec{\zeta}) \gamma_{\alpha\beta}(\vec{\eta}) \sqrt{a} dy + \frac{\varepsilon^3}{3} \int_{\omega} a^{\alpha\beta\sigma\tau} \rho_{\sigma\tau}(\vec{\zeta}) \rho_{\alpha\beta}(\vec{\eta}) \sqrt{a} dy,$$
$$f(\vec{\eta}) := \int_{\omega} p^i \eta_i \sqrt{a} dy,$$

problem (1) can be rewritten as follows:

$$\begin{cases}
Find \ \vec{\zeta} \in \vec{V}_K(\omega) := \{\vec{\zeta} = (\zeta_i) \in H^1(\omega) \times H^1(\omega) \times H^2(\omega); \zeta_i = \partial_n \zeta_3 = 0 \ on \ \gamma_0\}, \\
such that \quad a(\vec{\zeta}, \vec{\eta}) = f(\vec{\eta}), \quad \forall \vec{\eta} \in \vec{V}_k(\omega).
\end{cases}$$
(2)

Let the space  $\vec{V}_k(\omega)$  be equipped with the following norm:

$$\|\vec{\eta}\|_{\vec{V}_{K(\omega)}} = \sum_{\alpha=1}^{2} \|\vec{\eta_{\alpha}}\|_{H^{1}(\omega)} + \|\vec{\eta_{3}}\|_{H^{2}(\omega)}.$$

Since the bilinear form  $a(\cdot, \cdot)$  is  $\vec{V}_k(\omega)$  – elliptic (cf. [20]), the variational problem (2) has one and only one solution by Lax-Milgram Theorem (cf., e.g., [29]).

# 2.3 Numerical methods

The unknown variable is discretized by finite element methods (FEMs) (cf. [21] and [30]). To be more specific, given a triangulation  $\mathcal{T}_h$  of the domain  $\bar{\omega}$  (henceforth assumed to be polygonal) made of triangles denoted  $\mathbb{K} \in \mathcal{T}_h$ , we use a  $P_1$  triangle to approximate the tangential components  $\zeta_{\alpha}$  of the sought displacement vector field, and a Hsieh–Clough–Tocher triangle (i.e., HCT triangle), for approximating the normal component  $\zeta_3$  of the sought displacement vector field.

More specifically, we let

$$\vec{V}_h := V_{h1} \times V_{h2} \times V_{h3},$$

where

 $V_{h\alpha} := \{ \eta_h \in C^0(\bar{\omega}); \ \eta_h|_{\mathbb{K}} \in P_1(\mathbb{K}) \text{ for each } \mathbb{K} \in \mathcal{T}_h, \eta_h = 0 \text{ on } \gamma_0 \},$   $V_{h3} := \{ \eta_h : \bar{\omega} \to \mathbb{R}; \ \eta_h|_{\mathbb{K}_i} \in P_3(\mathbb{K}_i), \text{ for all } 1 \leq i \leq 3 \text{ and for each } \mathbb{K} \in \mathcal{T}_h,$   $\eta_h \text{ is } C^1\text{--continuous at each interior vertex,}$   $\partial_n \eta_h \text{ is continuous at each mid--point of each interior edge,}$ 

 $\eta_h = 0$  at each vertex that belongs to  $\gamma_0$ ,  $\partial_n \eta_h = 0$  at each mid-point of an edge that belongs to  $\gamma_0$ ,

where the notation  $P_k(\mathbb{K}), k \geq 1$ , designates the space formed by the restriction to a triangle  $\mathbb{K} \in \mathcal{T}_h$  of all the polynomials of degree  $\leq k$  in the two variables, with  $\mathbb{K}_i, i = 1, 2, 3$  defining a subdivision of  $\mathbb{K}$  into three triangles.

Then the finite element approximation to problem (2) is as follows:

$$\begin{cases} Find \ \vec{\zeta_h} \in \vec{V_h} \\ such \ that \ \ a(\vec{\zeta_h}, \vec{\eta_h}) = f(\vec{\eta_h}), \quad \forall \vec{\eta_h} \in \vec{V_h}. \end{cases}$$
 (3)

where the bilinear form a and the linear form f are defined in the proof of Theorem 2.1. We define the norms  $\|\cdot\|_{\vec{V}_h}$  on the space  $\vec{V}_h$  by

$$\|\vec{\eta}_h\|_{\vec{V}_h} := \sum_{\alpha} \|\vec{\eta}_{\alpha h}\|_{H^1(\omega)} + \|\eta_{3h}\|_{H^2(\omega)},$$

for each  $\vec{\eta}_h = (\eta_{1h}, \eta_{2h}, \eta_{3h}) \in \vec{V}_h$ .

Combining Lax-Milgram Theorem and the error estimate established in the monograph of Bernadou (cf. [21], page 71), we obtain the following theorem.

**Theorem 2.2.** Let the assumptions be the same as in Theorem 2.1. Then, the variational problems (3) has an unique solution. Let  $\vec{\zeta}$  and  $\vec{\zeta}_h$  denote the solutions to problems (2) and (3), respectively. Then, there exists a constant C, independent of h, such that  $\|\vec{\zeta} - \vec{\zeta}_h\|_{\vec{V}_h} \leq Ch$ .

# 3 Numerical experiments

The mitral valve is a cardiac valve connecting the left atrium and the left ventricle and contains an annulus, two leaflets, papillary muscles and chordae tendineae. The two valve leaflets are designated as the anterior leaflet and the posterior leaflet, the latter of which has three subregions.

For each leaflet of human mitral valve, the middle surface S is a portion of elliptic cylindrical shell when the mitral valve is fully open [15]. In terms of curvilinear coordinates, the surface S is described by the mapping  $\vec{\theta}$  defined by

$$\vec{\theta}(y_1, y_2) = (m\cos y_1, n\sin y_1, ly_2),$$

where  $y_1 \in [0, 2\pi]$ ,  $ly_2 \in [h_1(y_1), h_2(y_1)]$ , m, n,  $h_1(y_1)$  and  $h_2(y_1)$  represent the lengths of the semi-major axis, semi-minor axis, the height of the lower and upper boundaries, respectively, of the elliptic cylinder.

Then, the covariant basis of the tangent plane to S at  $\vec{\theta}(y)$  is

$$\vec{a}_1(y_1, y_2) = \partial_1 \vec{\theta}(y_1, y_2) = (-m \sin y_1, n \cos y_1, 0),$$
$$\vec{a}_2(y_1, y_2) = \partial_2 \vec{\theta}(y_1, y_2) = (0, 0, l).$$

From the definition of  $\vec{a}_3$ , we have

$$\vec{a}_3(y_1, y_2) := \frac{\vec{a}_1 \times \vec{a}_2}{|\vec{a}_1 \times \vec{a}_2|} = \left(\frac{n \cos y_1}{\sqrt{n^2 \cos^2 y_1 + m^2 \sin^2 y_1}}, \frac{m \sin y_1}{\sqrt{n^2 \cos^2 y_1 + m^2 \sin^2 y_1}}, 0\right).$$

Then, the covariant components of the metric tensor are given by

$$a_{11} = \vec{a}_1 \cdot \vec{a}_1 = m^2 \sin^2 y_1 + n^2 \cos^2 y_1, \qquad a_{21} = a_{12} = 0, \qquad a_{22} = l^2.$$

Thus,

$$a := \det(a_{\alpha\beta}) = \begin{vmatrix} a_{11} & a_{12} \\ a_{21} & a_{22} \end{vmatrix} = l^2(m^2 \sin^2 y_1 + n^2 \cos^2 y_1).$$

Since  $(a^{\alpha\beta}) = (a_{\alpha\beta})^{-1}$ , the contravariant components of the metric tensor are given by

$$a^{11} = \frac{1}{m^2 \sin^2 y_1 + n^2 \cos^2 y_1}, \qquad a^{21} = a^{12} = 0, \qquad a^{22} = \frac{1}{l^2}.$$

Hence,

$$\vec{a}^1 = a^{11}\vec{a}_1 = \left(\frac{-m\sin y_1}{m^2\sin^2 y_1 + n^2\cos^2 y_1}, \frac{n\cos y_1}{m^2\sin^2 y_1 + n^2\cos^2 y_1}, 0\right),$$
$$\vec{a}^2 = a^{22} \cdot \vec{a}_2 = \left(0, 0, \frac{1}{I}\right).$$

Since

$$\partial_1 \vec{a}_1 = (-m\cos y_1, -n\sin y_1, 0),$$
  
 $\partial_1 \vec{a}_2 = \partial_2 \vec{a}_1 = \partial_2 \vec{a}_2 = (0, 0, 0),$ 

the covariant and mixed components of the second fundamental form of S are given by

$$b_{11} = \vec{a}_3 \cdot \partial_1 \vec{a}_1 = \frac{-mn}{\sqrt{n^2 \cos^2 y_1 + m^2 \sin^2 y_1}},$$

$$b_{12} = b_{21} = b_{22} = 0,$$

$$b_1^1 = \frac{-mn}{(m^2 \sin^2 y_1 + n^2 \cos^2 y_1)^{\frac{3}{2}}}, \quad b_1^2 = b_2^1 = b_2^2 = 0.$$

Then, the Christoffel symbols of S are given by

$$\Gamma_{11}^{1} = \vec{a}^{1} \cdot \partial_{1} \vec{a}_{1} = \frac{(m^{2} - n^{2}) \sin y_{1} \cos y_{1}}{m^{2} \sin^{2} y_{1} + n^{2} \cos^{2} y_{1}},$$

$$\Gamma_{12}^{1} = \Gamma_{21}^{1} = \Gamma_{22}^{1} = 0,$$

$$\Gamma_{11}^{2} = \Gamma_{12}^{2} = \Gamma_{21}^{2} = \Gamma_{22}^{2} = 0.$$

According to [31], we take the value of the Young's modulus E as

$$E = 4 \times 10^6 \text{Pa},\tag{4}$$

and of the Poisson ratio as

$$\nu = 0.45. \tag{5}$$

Since the Lamé constants, the Poisson ratio and the Young modulus are related by the following equations (cf. e.g. [32]):

$$\lambda = \frac{E\nu}{(1+\nu)(1-2\nu)}, \mu = \frac{E}{2(1+\nu)},\tag{6}$$

plugging (4) and (5) into (6) yields

$$\lambda = 3.1 \times 10^6 \text{Pa}, \ \mu = 3.45 \times 10^5 \text{Pa}.$$

### 3.1 Anterior leaflet

In this paper, based on the theoretical research presented in [15], the middle surface S of the mitral valve when it is fully open is a portion of elliptic cylindrical shell (cf. Fig. 1): the parametric equation of the anterior mitral leaflet is that of equation (7) below:

$$\vec{\theta}(y_1, y_2) = (1.4\cos y_1, 1.04\sin y_1, 2.4y_2),\tag{7}$$

where  $y_1 \in [0, \pi], y_2 \in [0, siny_1].$ 



Figure 1: Anterior leaflet of the mitral valve

The domain  $\omega$  is defined by

$$\omega := \{(y_1, y_2) \in \mathbb{R}^2; \ y_1 \in [0, \pi], y_2 \in [0, \sin y_1]\},\$$

and the clamped boundary is defined as the image by  $\vec{\theta}$  of the set

$$\gamma_0 := \{ (y_1, y_2) \in \mathbb{R}^2; \ y_1 \in [0, \pi], \ y_2 = 0 \}.$$

Let the external forces be defined by  $p^1 = p^2 = 0$ , and  $p^3 = 1.5$ mmHg (cf. [11]). We carried out numerical experiments with four different meshes, comprising of  $16 \times 20$ ,  $32 \times 40$ ,  $64 \times 80$ , and  $128 \times 160$  as shown on Fig. 2 (cf. A1, B1, C1, D1). The Fig. 2 (cf. A2, B2, C2, D2) shows the distribution of the displacement of the anterior leaflet, when the anterior annular (the blue region on the top of each picture) is fixed, and the maximum deformation appears on the red region. As expected, the deformation of different meshes is similar when the mesh is ever smaller.

In order to further analyse the numerical results, we computed the maximum and the minimum of the three components of displacement  $(\zeta_1, \zeta_2, \zeta_3)$  on different meshes in Table 1. Obviously, the maximum and minimum errors of the three displacement components under different meshes are very small. The results in Fig.2 and Table 1 suggest that the finite element discrete scheme is stable and convergent for the proposed Koiter's model for elliptic cylindrical shell.

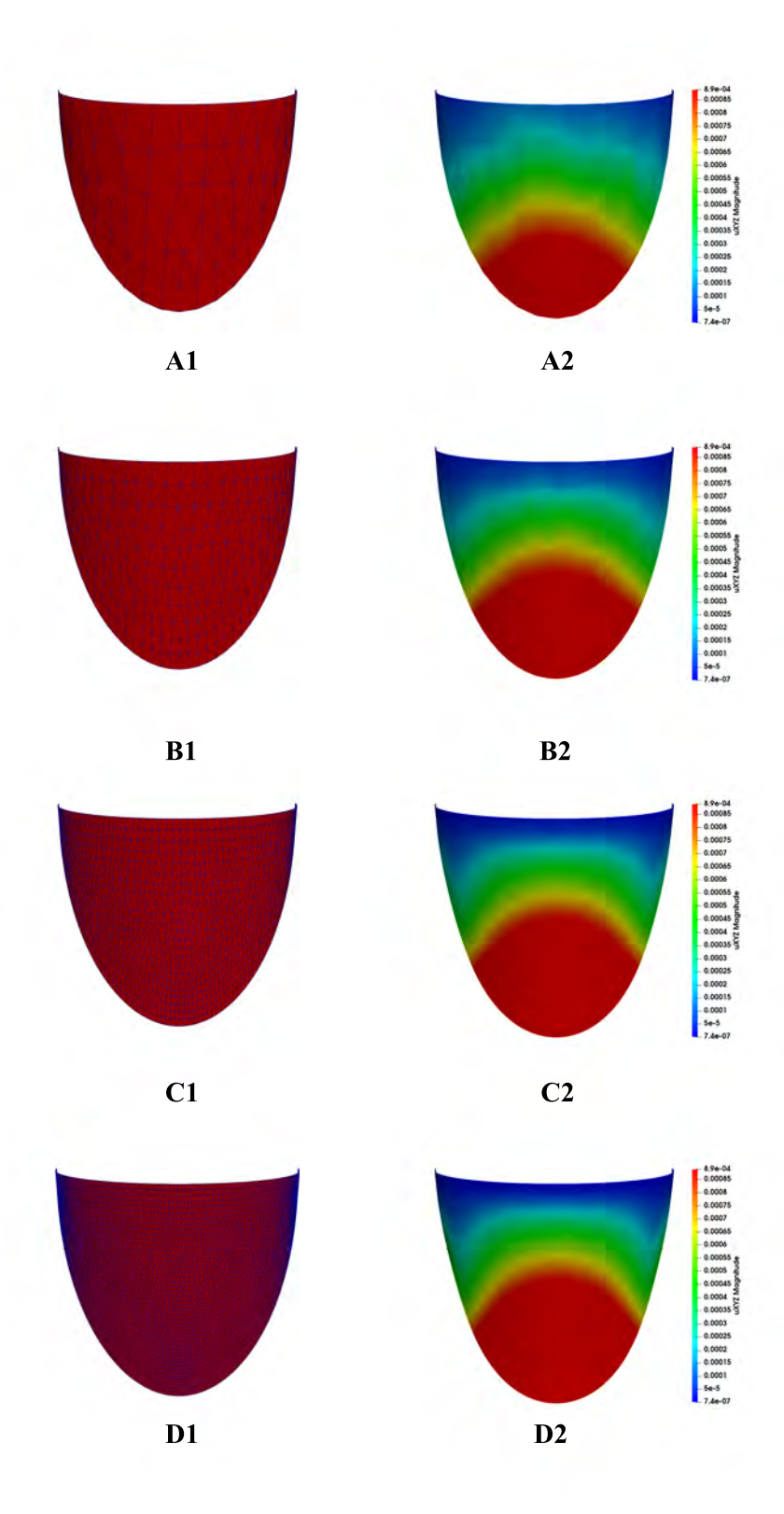


Figure 2: Numerical results on different meshes for the anterior leaflet

	mesh steps				
	$\frac{1}{20}$	$\frac{1}{40}$	$\frac{1}{80}$	1 160	
$\zeta_{1max}/10^{-6} \text{m}$	6.14517	7.85437	8.9569	9.38467	
$\zeta_{1min}/10^{-6} {\rm m}$	-6.15737	-7.87631	-8.95581	-9.38565	
$\zeta_{2max}/10^{-6} {\rm m}$	1.9829	2.60384	2.89493	3.01557	
$\zeta_{2min}/10^{-6} {\rm m}$	-3.26868	-4.23734	-4.82134	-5.03315	
$\zeta_{3max}/10^{-3} {\rm m}$	1.77949	2.68110	3.218720	3.463040	
$\zeta_{3min}/10^{-3} {\rm m}$	-1.80165	-2.504780	-3.442770	-3.764220	
Triangles	126	480	1948	7790	
Vertices	82	277	1047	4040	

Table 1: Comparison of the numerical results for the anterior leaflet on different meshes.

#### 3.2 Posterior leaflet

According to reference [15], the parametric equations for the three subregions (P1, P2, P3) of the posterior leaflet presented in the paper are as follows:

P1: 
$$\vec{\theta}(y_1, y_2) = (1.4 \cos y_1, 2.11 \sin y_1, 1.1y_2),$$

where  $y_1 \in \left[\pi, \frac{35\pi}{27}\right), y_2 \in U(y_1) = \left[0, \sin\left(3y_1 - 3\pi\right)\right),$ 

P2: 
$$\vec{\theta}(y_1, y_2) = (1.4 \cos y_1, 2.11 \sin y_1, 1.4y_2)$$

where 
$$y_1 \in \left[\frac{35\pi}{27}, \frac{31\pi}{18}\right), y_2 \in U(y_1) = \left[\frac{11}{14}\sin\frac{\pi}{9}, \frac{11}{14}\sin\frac{\pi}{9} + \left(1 - \frac{11}{14}\sin\frac{\pi}{9}\right)\sin\left[\frac{54}{23}(y_1 - \frac{35\pi}{27})\right]\right),$$

P3: 
$$\vec{\theta}(y_1, y_2) = (1.4 \cos y_1, 2.11 \sin y_1, 1.1y_2),$$

where 
$$y_1 \in \left[\frac{31\pi}{18}, 2\pi\right), y_2 \in U(y_1) = \left[0, \sin\frac{16}{5}(2\pi - y_1)\right).$$

where  $y_1 \in \left[\frac{31\pi}{18}, 2\pi\right), y_2 \in U(y_1) = \left[0, \sin\frac{16}{5}(2\pi - y_1)\right)$ . We assume that the middle surface S of the posterior leaflet is a portion of an elliptic cylindrical shell when it is fully open, as indicated in Fig. 3.



Figure 3: Posterior leaflet of the mitral valve

The domain  $\omega$  of the curvilinear coordinates on S is defined by

$$\omega := \{ (y_1, y_2) \in \mathbb{R}^2; \ y_1 \in [\pi, 2\pi], y_2 \in U(y_1) \},\$$

and the clamped boundary is defined as the image by  $\vec{\theta}$  of the set

$$\gamma_0 := \{ (y_1, y_2) \in \mathbb{R}^2; \ y_1 \in [\pi, 2\pi], \ y_2 = 0 \}.$$

The calculations are made on four meshes, comprising of  $20 \times 20 \times 20 \times 30$ ,  $40 \times 40 \times 40 \times 10^{-5}$  $40 \times 60, 80 \times 80 \times 80 \times 120, \text{ and } 160 \times 160 \times 160 \times 240 \text{ as shown on Fig. 4 (cf. A1,}$ 

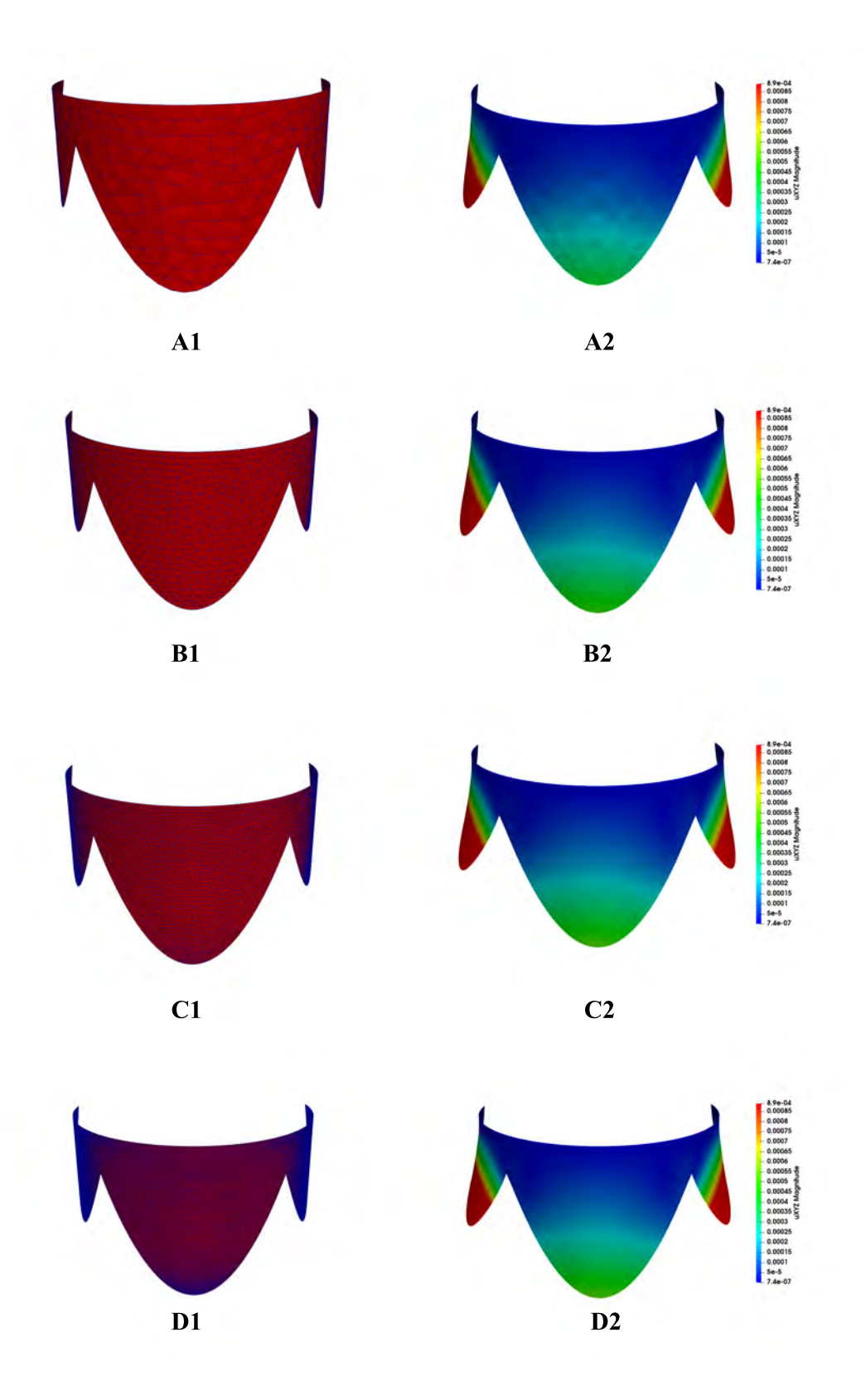


Figure 4: Numerical results on the different meshes for the posterior leaflet

B1, C1, D1). The right side of Fig. 4 (cf. A2, B2, C2, D2) shows the distribution of the displacement of the posterior leaflet on the corresponding mesh after the deformation, when the posterior annular is fixed. Then, we computed maximum and minimum of the three components of displacement  $(\zeta_1, \zeta_2, \zeta_3)$  on different meshes in Table 2.

Table 2: Comparison of the numerical results for the posterior leaflet on different mesl	Table 2:	Comparison	of the numerica	l results for the	posterior leaflet	on different meshe
--	----------	------------	-----------------	-------------------	-------------------	--------------------

	mesh steps				
	$\frac{1}{30}$	$\frac{1}{60}$	$\frac{1}{120}$	$\frac{1}{240}$	
$\zeta_{1max}/10^{-6} \text{m}$	3.78129	4.34080	4.50680	4.55608	
$\zeta_{1min}/10^{-6} {\rm m}$	-4.04611	-4.68564	-4.91010	-4.97725	
$\zeta_{2max}/10^{-7} {\rm m}$	3.55841	4.65556	5.18586	5.40142	
$\zeta_{2min}/10^{-7} {\rm m}$	-7.40491	-8.80006	-9.33077	-9.48805	
$\zeta_{3max}/10^{-3} \text{m}$	3.00960	2.68110	3.90270	3.91008	
$\zeta_{3min}/10^{-3} {\rm m}$	-2.87216	-3.70058	-3.81714	-3.94049	
Triangles	414	1658	6628	26444	
Vertices	253	920	3495	13583	

The fact that the minor axis of the posterior annulus and the major axis of the anterior annulus are equal in length, provides the possibility of coupling the two leaflets. The numerical results for this coupling are shown in Fig. 5.

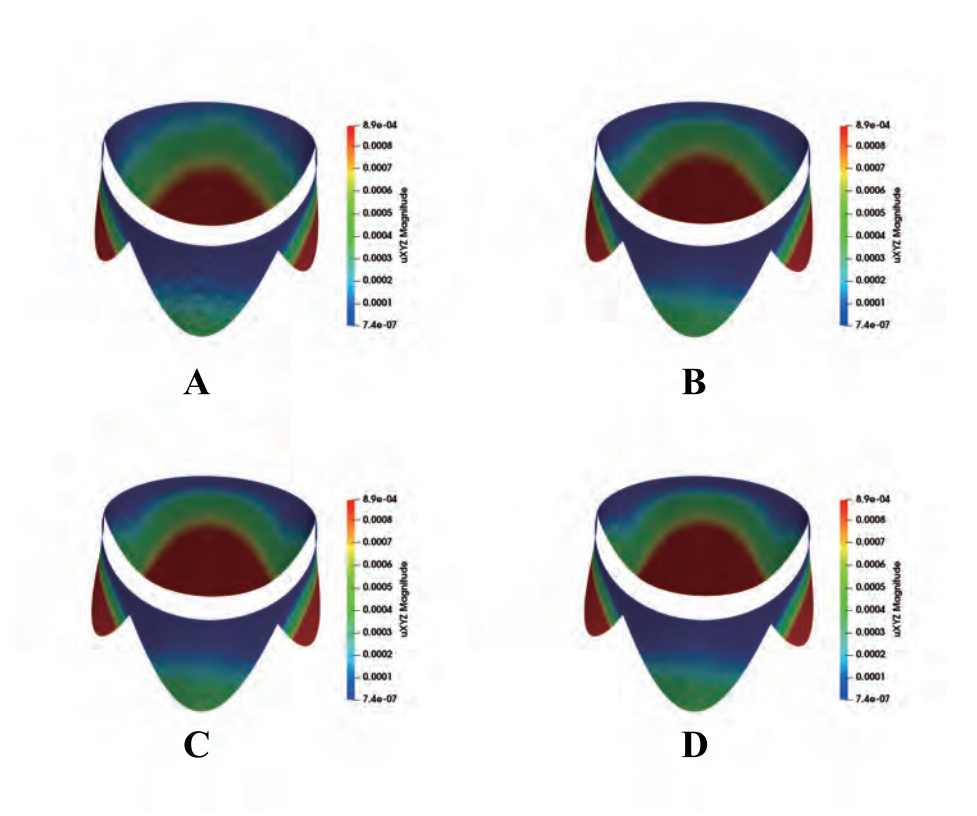


Figure 5: Numerical results on different meshes

# 4 Conclusions

In this study, a mathematical model is established (a Koiter's type model) for mitral valve leaflets, and numerical methods are presented, namely conforming finite element (P1 and HCT triangles), to compute the deformation of the mitral valve. The numerical results suggest that the proposed mathematical models could simulate the human mitral valve well. The results from this study will be extended to the dynamic model for the human mitral valve during a cardiac cycle in a forthcoming paper.

# References

- [1] M. S. Sacks and A. P. Yoganathan, Heart valve function: a biomechanical perspective, Philosophical Transactions of the Royal Society of London, 362 (2007), 1369–1391.
- [2] E. Weinberg and M. Kaazempur-Mofrad, A large-strain finite element formulation for biological tissues with application to mitral valve leaflet tissue mechanics. Journal of Biomechanics, 39 (2006), 1557–1561.
- [3] E. Weinberg and M. Kaazempur-Mofrad, A finite shell element for heart mitral valve leaflet mechanics, with large deformations and 3d constitutive material model, Journal of Biomechanics, 40 (2007), 705–711.
- [4] V. Prot, R. Haaverstad and B. Skallerud, Finite element analysis of the mitral apparatus: annulus shape effect and chordal force distribution, Biomech Model Mechanobiol, 8 (2009), 43–55.
- [5] P. F. Dal, G. C. Donzella and M. Schreiber, Structural effects of an innovative surgical technique to repair heart valve defects, Journal of Biomechanics, 38 (2005), 24–60.
- [6] K. S. Kunzelman, R. P. Cochran, C. Chuong, W. S. Ring, E. D. Verrier and R. D. Eberhart, Finite element analysis of the mitral valve, Journal of Heart Valve Disease, 2 (1993), 326–340.
- [7] K. S. Kunzelman, R. P. Cochran, E. D. Verrier and R. D. Eberhart, Anatomic basis for mitral valve modeling, Journal of Heart Valve Disease, 3 (1994), 491–496.
- [8] K. S. Kunzelman, R. D. Eberhart and R. P. Cochran, Fluid-structure interaction models of the mitral valve: function in normal and pathological states, Philosophical Transactions of the Royal Society of London, 362 (2007), 1393–1406.
- [9] K. H. Lim, J. H. Yeo and C. M. Duran, Three-dimensional asymmetrical modeling of the mitral valve: a finite element study with dynamic boundaries, Journal of Heart Valve Disease, 14 (2005), 386–392.
- [10] D. R. Einstein, F. D. Pin, X. Jiao, A. P. Kuprat, J. P. Carson, K. S. Kunzelman, R. P. Cochran, J. M. Guccione and M. B. Ratcliffe, Fluid-Structure Interactions of the Mitral Valve and Left Heart: Comprehensive Strategies, Past, Present and Future,

- International Journal for Numerical Methods in Biomedical Engineering, 26 (2010), 348–380.
- [11] S. Marco, V. Emiliano and R. Alberto, Mitral valve finite element modeling: implications of tissues' nonlinear response and annular motion, Journal of Biomechanical Engineering, 131 (2009), 121010.
- [12] H. Gao, N. Qi, L. Feng, X. Ma, M. Danton, C. Berry and X. Luo, Modelling Mitral Valvular Dynamics - current trend and future directions, International Journal for Numerical Methods in Biomedical Engineering, 23 (2016), e2858.
- [13] X. Ma, H. Gao, B. E. Griffith, C. Berry and X. Luo, Image-based fluid-structure interaction model of the human mitral valve, Computers and Fluids, 71 (2013), 17–425.
- [14] L. Cai, Y. Wang, H. Gao, X. Ma, G. Zhu, R. Zhang, X. Shen and X. Luo, Some effects of different constitutive laws on FSI simulation for the mitral valve, Scientific Reports, 9 (2019), 12753.
- [15] X. Shen, T. Wang, X. Cao and L. Cai, The geometric model of the human mitral valve, Plos One, 12 (2017), e0183362.
- [16] X. Shen, B. Lin, L. Cai and X. Cao, A geometric model for the human pulmonary valve in its fully open case, Plos One, 13(2018), e0199390.
- [17] X. Shen, Q. Yang, L. Li, L. Cai and X. Cao, An Elastic Shell Model for the Human Tricuspid Valve, Acta Mathematicae Applicatae Sinica, 35 (2019), 111–128.
- [18] W. T. Koiter, On the foundations of the linear theory of thin elastic shells, Proceedings of the Koninklijke Nederlandse Academie van Wetenschappen, B73 (1970), 169-195.
- [19] W. T. Koiter, A consistent first approximation in the general theory of thin elastic shells, Proc.Sympos.Thin Elastic Shells, (1960) 12-13.
- [20] P. G. Ciarlet and V. Lods, Asymptotic analysis of linearly elastic shells. III. A justification of Koiter's shell equations, Archive for Rational Mechanics and Analysis, 136 (1996), 191-200.
- [21] M. Bernadou, Finite element methods for thin shell problems, Wiley, New York, 1996.
- [22] X. Shen, K. Li and Y. Ming, The ODEs forms of linearly elastic shell model and its numerical computing, Applied Mathematical Modelling, 36 (2012), 3320-3328.
- [23] X. Shen and H. Li, The time-dependent Koiter model and its numerical computation, Applied Mathematical Modelling, 55 (2018), 131-144.

- [24] X. Shen, J. Jia, S. Zhu, H. Li, L. Bai, T. Wang and X. Cao, The time-dependent generalized membrane shell model and its numerical computation, Computer Methods in Applied Mechanics and Engineering, 344 (2019), 54-70.
- [25] X. Shen, L. Piersanti and P. Piersanti, Numerical simulations for the dynamics of flexural shells, Mathematics and Mechanics of Solids, 25 (2020), 887-912.
- [26] X. Shen, Q. Yang, L. Li and Z. Gao, Numerical approximation of the dynamic Koiter's model for the hyperbolic parabolic shell, Applied Numerical Mathematics, 150 (2020), 194-205.
- [27] P. G. Ciarlet, Mathematical elasticity. Vol. III. Theory of shells, North-Holland, Amsterdam, 2000.
- [28] P. G. Ciarlet, An Introduction to Differential Geometry with Applications to Elasticity, Springer, Dordrecht, 2005.
- [29] L. C. Evans, Partial differential equations, American Mathematical Society, 1998.
- [30] P. G. Ciarlet, The Finite Element Method for Elliptic Problems. Volume 4, North-Holland Amsterdam, 1978.
- [31] K. D. Lau, V. Diaz, P. Scambler and G. Burriesci, Mitral valve dynamics in structural and fluid-structure interaction models, Medical Engineering and Physics, 32 (2010), 1057-1064.
- [32] J. L. Lions and E. Magenes, Non-Homogeneous Boundary Value Problems and Applications: Volume II. Springer-Verlag, 1972.